Hindawi
International Journal of Aerospace Engineering
Volume 2018, Article ID 9235124, 11 pages
https://doi.org/10.1155/2018/9235124

Research Article

Design of Three-Dimensional Path Following Guidance Logic

Sungsu Park

Department of Aerospace Engineering, Sejong University, Seoul 05006, Republic of Korea

Correspondence should be addressed to Sungsu Park; sungsu@sejong.ac.kr

Received 14 April 2018; Revised 22 May 2018; Accepted 30 May 2018; Published 21 June 2018

Academic Editor: Christian Circi

This paper presents a three-dimensional path following guidance logic. The proposed guidance logic is composed of the guidance law and the motion strategy of virtual target along the desired path. The guidance law makes a vehicle purse the virtual target, and the motion strategy explicitly specifies the motion of virtual target by introducing the concept of the projection point and the tangentially receding distance. The proposed logic is simple and efficient and yet provides precise path following. Numerical simulations are performed to demonstrate the effectiveness of the proposed guidance logic.

1. Introduction

Path following problem is to design a guidance law that will make a vehicle to follow a desired path. The desired path usually consists of consecutive segments which are comprised of circular arc and straight-line path. Path following problem has been a research topic over the last two decades, and many methods have been developed in response to the need for efficient and reliable path following guidance systems. Most of the methods have been developed for the paths in planar motion.

The path following guidance law specifies command acceleration that is applied to the vehicle, and the control law of the vehicle follows the command generated by the guidance law. There are many control methods [1] for implementing these commands in the vehicle. Although guidance loop and control loop can be designed separately, there are alternative methods for combining both guidance and control loops [2, 3]. However, these methods are usually more complex to use in real applications [4]. This paper is concerned only with guidance loop.

Conventional approach for path following is based on the proportional-integral-derivative (PID) control. This approach relies on the cross-track error, and if the error is small, then linear feedback on the cross-track error provides good performance. Other approach is to construct vector fields surrounding the path so that the vehicle converges to the desired path along the vector field [5, 6]. Global convergence is proved, but this method is not applicable to three-dimensional space paths. Recent common approach [7–13] is rewriting the path following problem as the classical line-of-sight guidance problem by specifying a moving virtual target along the desired path. This approach generates a simple guidance law, yet can compensate a large deviation from the desired path. However, the position of virtual target is not easy to determine, and the initial distance between the vehicle and the desired path should be less than the specified distance. Some methods in this approach are still for the paths in planar motion [9–13].

Motivated by these observations, a new three-dimensional path following guidance logic is proposed in this paper. The proposed guidance logic is equally applicable to two primitive path types in three-dimensional space: straight-line path and circular path, and might be extendable to any smooth path. Similar to the methods in [7–13], the proposed guidance logic also uses a moving virtual target on the desired path; however, the proposed logic explicitly specifies the motion of virtual target by introducing the concept of the projection point and the tangentially receding distance. The proposed logic is simple and efficient, yet provides precise path following.

This paper is organized as follows. In the next section, a three-dimensional engagement geometry of a vehicle and virtual target is presented to formulate the problem, and the guidance law is proposed to pursue this virtual target. In Section 3, the motion of virtual target is specified explicitly

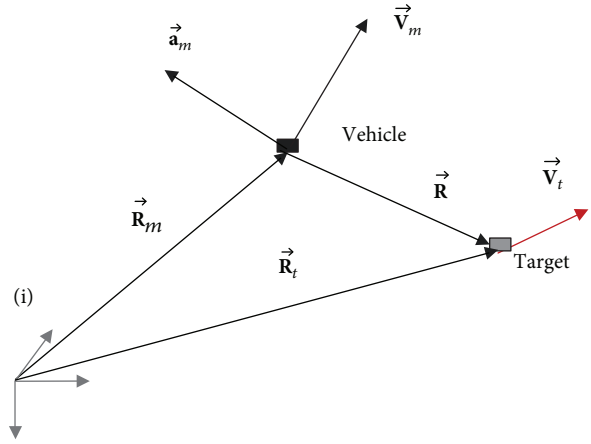

Figure 1: Three-dimensional vehicle/target engagement.

according to the position and velocity vectors of the vehicle and the geometry of the desired path. Some linearized stability analyses are also performed. In Section4, numerical simulation results are provided to demonstrate the performance of the proposed guidance logic. Conclusions are given in Section 5.

2. Design of Guidance Law

The proposed path following guidance logic is composed of the guidance law and the motion strategy of virtual target. In this section, the guidance law is firstly described. The guidance law generates command acceleration that is applied to the vehicle.

2.1. Engagement Kinematics. Figure 1 illustrates the overall kinematics of three-dimensional engagement between the vehicle and the virtual target on the desired path. The inertial frame is represented by $\{i\}$. $\vec{\mathbf{R}}_m$ and $\vec{\mathbf{V}}_m$ are the position and velocity vectors of the vehicle, respectively; $\vec{\mathbf{a}}_m$ represents the command acceleration vector which is assumed to be perpendicular to the velocity vector of vehicle; and $\vec{\mathbf{R}}$ is the relative position vector or line-of-sight (LOS) vector from the vehicle to the target. The position vector $\vec{\mathbf{R}}_t$ and velocity vector $\vec{\mathbf{V}}_t$ of the virtual target will be determined in further sections.

In this framework, the path following guidance law leads the vehicle to pursue a moving virtual target, while the interception of a target is not a goal as in the missile guidance law.

The guidance law in this paper issues an acceleration command which is perpendicular to the velocity vector. Therefore, the speed of the vehicle is not to be constrained by the guidance law but allowed to be controlled independently. This is because path following is required for a vehicle to follow a desired path without any temporal specifications. Note that, on the other hand, trajectory tracking is required to track a time-parameterized trajectory [14].

2.2. Guidance Law. In a missile community, pure proportional navigation guidance (PPNG) law has been widely used for targeting an enemy target [15]. PPNG tends to keep a constant LOS angle and eventually delivers a missile into a target if the missile speed is sufficiently larger than that of the target. However, PPNG is not considered in path following problem since a constant LOS angle does not guarantee path following, and moreover the relative distance between the target and vehicle is typically kept constant in path following problem.

Pursuit guidance (PG) law has also been used in the missile community. Although it is known to be suboptimal guidance law for intercept purpose [15], PG can direct the vehicle along the LOS irrespective of the vehicle and target velocities. Therefore, many PG and PG variants are used in recent path following studies with a moving virtual target concept.

In this paper, however, the combined PPNG and PG law is proposed as a path following guidance law as in (1).

$$\vec{\mathbf{a}}_m = N\frac{\left(\vec{R}\times\vec{\mathbf{V}}\right)}{R^2}\times\vec{V}_m - hN\frac{\left(\vec{R}\times\vec{V}_m\right)}{R^2}\times\vec{V}_m, \quad (1)$$

where $N>0$ and $h>0$ are proportional and pursuit gains, respectively; R represents the distance between the vehicle and target; and $\vec{\mathbf{V}} = \vec{V}_t - \vec{V}_m$ is the relative velocity vector. The first term of (1) is PPNG law and the second is PG law. Therein, the gain terms N and h determine the performance of path following and will be further investigated in the next section by using a linear analysis.

The reason of the addition of PPNG to PG is two folds. One is for enhancing damping for a straight-line path and the other is for providing the centripetal acceleration for a circular path. In this way, both paths are successfully followed.

The proof of convergence of PPNG and PG law in three-dimensional space is very difficult and complex mainly due to the much higher complexity of the three-dimensional pursuit dynamics than that of two-dimensional dynamics. Some sufficient conditions can be found in [16, 17] under which a vehicle guided by the three-dimensional guidance law can always intercept a target maneuvering arbitrarily with time-varying normal acceleration.

The next section determines the explicit motion of virtual target.

3. Design of Virtual Target Motion

In this section, the motion of virtual target is explicitly determined for two cases, straight-line path and circular path. The proposed positioning method for the virtual target is conceptually simple and extendible to any smooth path.

3.1. Straight-Line Path. The straight-line path is specified by two waypoint vectors $\vec{\mathbf{W}}_i$ and $\vec{\mathbf{W}}_{i+1}$ and a unit direction vector $\hat{\mathbf{e}}_{t_i}$ along the straight-line segment connecting waypoints i and $i+1$ as shown in Figure 2. The waypoint vector is a position vector to a waypoint from the origin of inertial frame. The point D is the projection of the vehicle on the path, and R_0 is the receding distance of the virtual target computed along the path starting from D. In this way, the

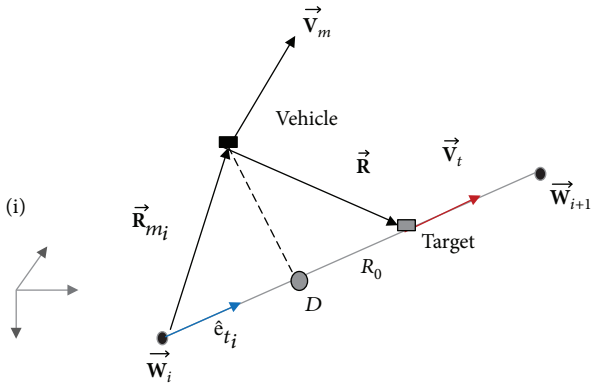

Figure 2: Straight path following.

virtual target is always ensured to be located on the path. In Figure 2, $\vec{\mathbf{R}}_{m_i} = \vec{R}_m - \vec{W}_i$ is the relative position vector of a vehicle from the waypoint i.

The speed of the virtual target is determined by the projection of the current velocity vector of a vehicle on the path. Therefore, the position and velocity vectors of the virtual target are computed as

$$\begin{aligned} \vec{\mathbf{R}}_t &= \vec{W}_i + \left(\vec{R}_{m_i} \cdot \hat{e}_{t_i}\right)\hat{e}_{t_i} + R_0 \hat{e}_{t_i}, \\ \vec{\mathbf{V}}_t &= \dot{\vec{R}}_t = \left(\vec{V}_m \cdot \hat{e}_{t_i}\right)\hat{e}_{t_i}. \end{aligned} \tag{2}$$

The receding distance R_0 between the virtual target and the projection point is the design choice of the proposed guidance logic. The influence of this value can be investigated by the linear analysis using similar method to [10]. Figure 3 shows a linearization situation and the relationship between the vehicle velocity vector $\vec{\mathbf{V}}_m$ and the relative velocity vector $\vec{\mathbf{V}}$, where d denotes the cross-track error.

Then, the guidance law of (1) becomes

$$a_m \approx N \frac{V_m^2}{R} \cos\alpha_2 \sin\alpha_1 + hN \frac{V_m^2}{R} \sin\alpha. \tag{3}$$

Assuming that the magnitudes of d/R_0 and $\alpha = \alpha_1 + \alpha_2$ are small,

$$\begin{aligned} R &\approx R_0, \\ \cos\alpha_2 &\approx 1, \\ \sin\alpha_1 &\approx \frac{\dot{d}}{V_m}, \\ \sin(\alpha_1 + \alpha_2) &\approx \frac{\dot{d}}{V_m} + \frac{d}{R_0}, \end{aligned} \tag{4}$$

then (3) can be written as

$$a_m \approx N \frac{V_m}{R_0}\dot{d} + hN \frac{V_m}{R_0}\dot{d} + hN \frac{V_m^2}{R_0^2} d. \tag{5}$$

Equation (5) resembles the proportional and derivative (PD) control and indicates that the two gains N and h and the ratio of vehicle speed V_m and the distance R_0 for the virtual target behave as the PD control gains. The first term of the right-hand side of the above equation is due to pure proportional navigation guidance (PPNG) law and the second and third terms pursuit guidance (PG) law. Thus, the PPNG law enhances the damping performance. Assuming further $a_m \approx -\ddot{d}$, (5) reduces to

$$\ddot{d} + N(1+h)\frac{V_m}{R_0}\dot{d} + hN\frac{V_m^2}{R_0^2} d = 0. \tag{6}$$

Equation (6) shows that the cross-track error dynamics is a second-order system, and the track error eventually goes to zero. The damping ratio and natural frequency are determined by PD control gains, which are $(N(1+h))/(2\sqrt{hN})$ and $\sqrt{hN}(V_m/R_0)$, respectively. For example, if $N = 1$ and $h = 2$ are chosen, then the damping ratio is 1.06 and the natural frequency is $\sqrt{2}(V_m/R_0)$.

The receding distance R_0 also plays a role as a look-ahead distance to detect the end of the path segment. As the vehicle moves, the virtual target also moves along the desired path which consists of consecutive segments. When the receding distance R_0 reaches the end of the current segment, a new virtual target position must be selected on the next segment to proceed to the next waypoint $\vec{W}_{i+2}$.

In this segment switching situation as shown in Figure 4, a new projection point D' on the next segment is firstly determined, and a new virtual target position is computed at a point on the next path segment that is R_0 distant from the new projection point D'. This segment switching logic is very simple and practical compared to the previous methods in the literatures since no additional methods are required to ensure that the virtual target always exists on the new path segment.

3.2. Circular Path. The circular path is specified by a unit vector $\hat{\mathbf{e}}_{\text{rot}}$ for indicating the direction of rotation, a position vector $\vec{\mathbf{P}}_c$ pointing to the centre of the circle, and the circle radius R_c, as shown in Figure 5. The two waypoint vectors $\vec{\mathbf{W}}_i$ and $\vec{\mathbf{W}}_{i+1}$ indicate the start and end points of the circular path.

For the circular path following case, a virtual target is proposed to be positioned on the tangent line at the point D with a tangential distance R_0 ahead of that point, where the point D is the projection point of the vehicle position onto the circular path. Note that the virtual target is not positioned on the circular path. In this way, the positioning method of the virtual target maintains consistency with the straight-line path case. Furthermore, this positioning method is very simple and practical compared to the previous methods in which the target is positioned at a point on the circular path, which is usually selected as an intersection point of the circular path and the reference distance from the vehicle [9–11].

In Figure 5, a unit direction vector $\hat{\mathbf{e}}_t$ represents a direction of tangent line at the projection point D, and $\vec{\mathbf{R}}_{\text{cm}}$ is a position vector from the centre of circle to the vehicle.

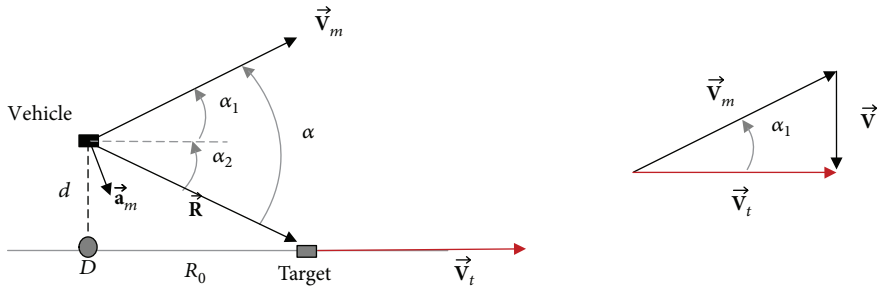

Figure 3: Linear model for straight-line path following.

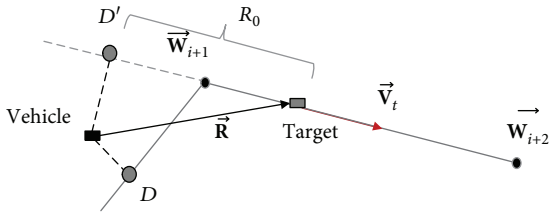

Figure 4: Path segment switching.

Then, the position and velocity vectors of the virtual target are expressed as

$$\vec{\mathbf{R}}_t = R_c \hat{e}_d + R_0 \hat{e}_t + \vec{P}_c, \tag{7}$$

$$\vec{\mathbf{V}}_t = \dot{\vec{R}}_t = R_c \dot{\hat{e}}_d + R_0 \dot{\hat{e}}_t. \tag{8}$$

In (8), a unit direction vector $\hat{\mathbf{e}}_d$ represents a direction from the centre of the circle to the projection point D and is given by

$$\vec{R}_{\mathrm{cm}}^{\perp} = \vec{R}_{\mathrm{cm}} - \left(\vec{R}_{\mathrm{cm}} \cdot \hat{e}_{\mathrm{rot}}\right)\hat{e}_{\mathrm{rot}}, \tag{9}$$

$$\hat{\mathbf{e}}_d = \frac{\vec{R}_{\mathrm{cm}}^{\perp}}{|\vec{R}_{\mathrm{cm}}^{\perp}|}, \tag{10}$$

where $\vec{R}_{\mathrm{cm}}^{\perp}$ represents a projection of the vector $\vec{\mathbf{R}}_{\mathrm{cm}}$ onto the circle contained plane. The time derivative terms for the two unit direction vectors in (8) can be calculated by differentiating (10) as

$$\dot{\hat{e}}_d = \frac{\dot{\vec{R}}_{\mathrm{cm}}^{\perp}}{|\vec{R}_{\mathrm{cm}}^{\perp}|} - \frac{\left(\vec{R}_{\mathrm{cm}}^{\perp} \cdot \dot{\vec{R}}_{\mathrm{cm}}^{\perp}\right)\vec{R}_{\mathrm{cm}}^{\perp}}{\left|\vec{R}_{\mathrm{cm}}^{\perp}\right|^3}, \tag{11}$$

$$\dot{\vec{R}}_{\mathrm{cm}}^{\perp} = \vec{V}_m - \left(\vec{V}_m \cdot \hat{e}_{\mathrm{rot}}\right)\hat{e}_{\mathrm{rot}},$$

which can be further simplified as follows:

$$\dot{\hat{e}}_d = \frac{1}{\left|\vec{R}_{\mathrm{cm}}^{\perp}\right|}\left(\vec{V}_m \cdot \hat{e}_t\right)\hat{e}_t. \tag{12}$$

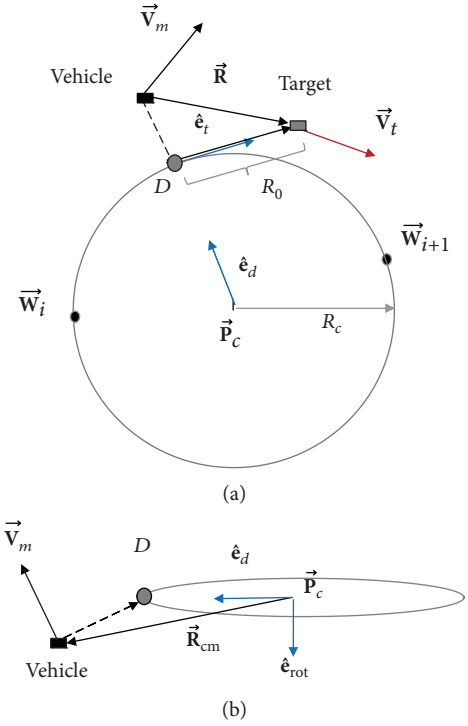

Figure 5: Circular path following. (a) Top view, (b) side view.

Since $\hat{\mathbf{e}}_t = \hat{e}_{\mathrm{rot}} \times \hat{e}_d$, differentiating it gives

$$\dot{\hat{e}}_t = \hat{e}_{\mathrm{rot}} \times \dot{\hat{e}}_d = -\frac{1}{\left|\vec{R}_{\mathrm{cm}}^{\perp}\right|}\left(\vec{V}_m \cdot \hat{e}_t\right)\hat{e}_d. \tag{13}$$

Substituting (12) and (13) to (8), the velocity vector of the virtual target can be computed as

$$\vec{\mathbf{V}}_t = \frac{R_c}{\left|\vec{R}_{\mathrm{cm}}^{\perp}\right|}\left(\vec{V}_m \cdot \hat{e}_t\right)\hat{e}_t - \frac{R_0}{\left|\vec{R}_{\mathrm{cm}}^{\perp}\right|}\left(\vec{V}_m \cdot \hat{e}_t\right)\hat{e}_d. \tag{14}$$

Note that unlike the straight-line path case, the velocity vector of the virtual target is not along the $\hat{\mathbf{e}}_t$ direction.

As a special case, if the motion of the vehicle initially begins on the circular path with the direction along the tangential unit vector $\hat{\mathbf{e}}_t$, that is,

$$\vec{\mathbf{R}}_m = R_c \hat{e}_d + \vec{P}_c, \vec{V}_m = V_m \hat{e}_t, \tag{15}$$

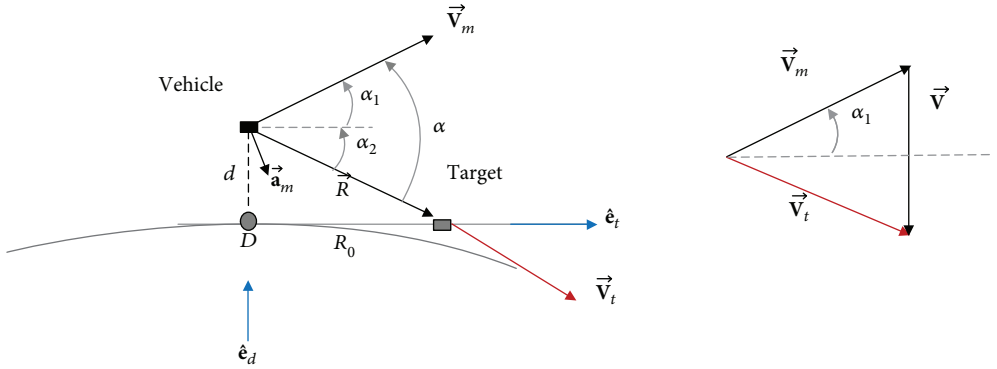

Figure 6: Linear model for circular path following.

then the target velocity vector and the relative position and velocity vectors are reduced to

$$\begin{aligned}\vec{\mathbf{V}}_t &= V_m \hat{e}_t - \frac{R_0 V_m}{R_c}\hat{e}_d,\\ \vec{\mathbf{R}} &= R_0 \hat{e}_t,\\ \vec{\mathbf{V}} &= -\frac{R_0 V_m}{R_c}\hat{e}_d,\end{aligned} \tag{16}$$

and the guidance law in (1) becomes

$$\vec{\mathbf{a}}_m = -N\frac{V_m^2}{R_c}\hat{e}_d. \tag{17}$$

Therefore, with a proportional gain of $N = 1$, the guidance law produces the command acceleration that is the same with the centripetal acceleration which is appropriate to follow the circle with radius R_c. Note that pursuit guidance (PG) law generates zero command acceleration, which means that PG law makes no contribution in this special case.

The tangentially receding distance R_0 between the virtual target and the projection point is also the design choice of the proposed guidance logic. The influence of this value can be investigated by the linear analysis. Figure 6 shows a linearization situation with assumption that the vehicle motion is perturbed from the initial circular path following motion. In Figure 6, d denotes the cross-track error, and the relationship between the vehicle velocity vector $\vec{\mathbf{V}}_m$ and the relative velocity vector $\vec{\mathbf{V}}$ is also shown.

Assuming that all the vectors are almost in the same plane which contains a circular path and the magnitudes of d/R_c and α_1 are small, then $\vec{R}_{cm}^{\perp} \approx \vec{R}_{cm}$ and $\dot{\vec{R}}_{cm}^{\perp} \approx \vec{V}_m$ are satisfied, and the relative velocity vector is approximately expressed as

$$\vec{\mathbf{V}} \approx -\frac{R_0 V_m}{R_c}\hat{e}_d. \tag{18}$$

Therefore, the guidance law of (1) becomes

$$a_m \approx N\frac{V_m^2 R_0}{R R_c}\cos\alpha_2 + hN\frac{V_m^2}{R}\sin\alpha. \tag{19}$$

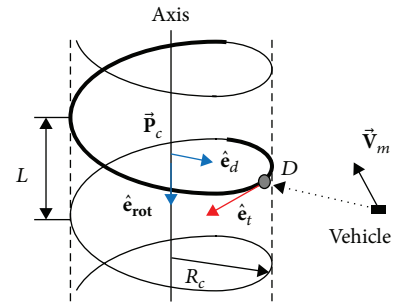

Figure 7: Helical path following.

Assuming also that the magnitudes of d/R_0 and $\alpha = \alpha_1 + \alpha_2$ are small,

$$\begin{aligned}R &\approx R_0,\\ \cos\alpha_2 &\approx 1,\\ \sin(\alpha_1+\alpha_2) &\approx \frac{\dot{d}}{V_m} + \frac{d}{R_0},\end{aligned} \tag{20}$$

then (19) can be written as

$$a_m \approx N\frac{V_m^2}{R_c} + hN\frac{V_m}{R_0}\dot{d} + hN\frac{V_m^2}{R_0^2}d. \tag{21}$$

Equation (21) resembles proportional and derivative (PD) control with the forcing term of $N(V_m^2/R_c)$. The first term of the right-hand side of the above equation is due to pure proportional navigation guidance (PPNG) law, and the second and third terms are due to pursuit guidance (PG) law. Thus, the PPNG law provides the centripetal acceleration, and the PG law plays a role as a PD control. Since the vehicle is approximately in circular motion, $a_m \approx (V_m^2/R_c) - \ddot{d}$ holds and (21) is reduced to

$$\frac{V_m^2}{R_c} = N\frac{V_m^2}{R_c} + \ddot{d} + hN\frac{V_m}{R_0}\dot{d} + hN\frac{V_m^2}{R_0^2}d. \tag{22}$$

Equation (22) implies that with a proportional gain of $N = 1$, the cross-track error dynamics is a second-order system and the track error eventually goes to zero. The damping

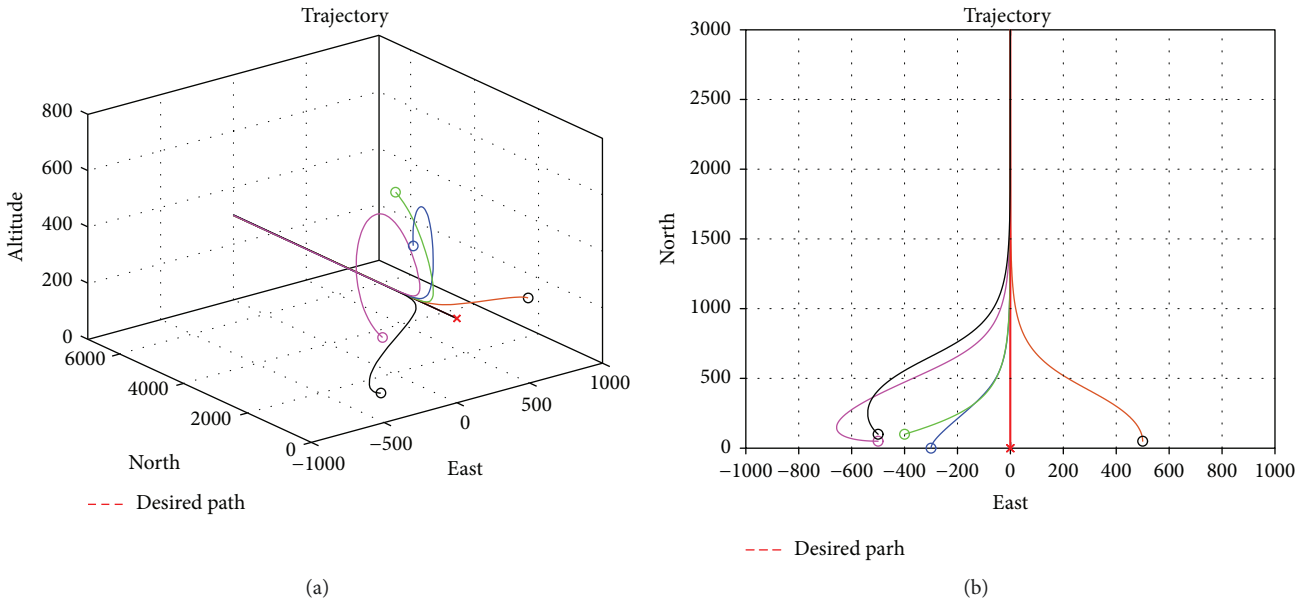

Figure 8: Straight-line path following for various initial conditions. (a) Three-dimensional view, (b) planar view.

ratio and natural frequency are determined by two guidance gains and the ratio of the vehicle speed and the tangentially receding distance R_0, which are $\sqrt{hN}/2$ and $\sqrt{hN}(V_m/R_0)$, respectively. For example, if $N = 1$ and $h = 2$ are chosen, then the damping ratio is $1/\sqrt{2}$ and the natural frequency is $\sqrt{2}(V_m/R_0)$.

The proposed strategy for specifying the motion of virtual target involves computations of position and velocity of the projection point and the receding point on the tangent line at the projection point, which depend on both the velocity of vehicle and the geometry of the desired path. Although more complex computations are expected than the straight-line or circular path, this is conceptually possible to any smooth path.

For example, in case of helical path defined on a vertical cylinder of radius R_c as shown in Figure 7, the position and velocity vectors of virtual target in (8) are modified as

$$\begin{aligned} \overrightarrow{\mathbf{R}}_t &= R_c \hat{e}_d + R_0 \hat{e}_t + \overrightarrow{\mathbf{P}}_c, \\ \overrightarrow{\mathbf{V}}_t &= R_c \dot{\hat{e}}_d + R_0 \dot{\hat{e}}_t + \dot{\overrightarrow{P}}_c, \end{aligned} \tag{23}$$

where $\overrightarrow{\mathbf{P}}_c$ is now a position vector pointing to the instantaneous centre of curvature at the point D. The time derivative of $\overrightarrow{\mathbf{P}}_c$ is given by a vertical component of the velocity vector of a vehicle as follows:

$$\dot{\overrightarrow{P}}_c = \left(\overrightarrow{V}_m \cdot \hat{e}_{\text{rot}}\right)\hat{e}_{\text{rot}}. \tag{24}$$

The time derivative of a unit direction vector $\hat{\mathbf{e}}_d$ in (12) is modified as

$$\dot{\hat{e}}_d = \frac{1}{\left|\overrightarrow{R}_{\text{cm}}^{\perp}\right|}\left(\overrightarrow{V}_m \cdot \hat{\mathbf{e}}_n\right)\hat{\mathbf{e}}_n, \tag{25}$$

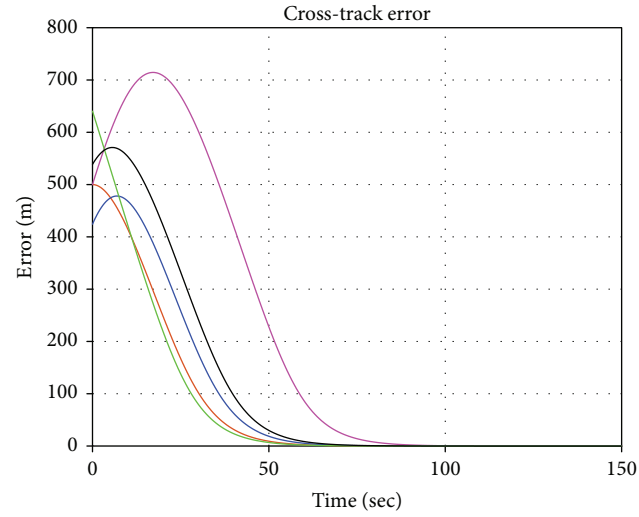

Figure 9: Cross-track errors.

where $\hat{\mathbf{e}}_n = \hat{e}_{\text{rot}} \times \hat{e}_d$ is a unit normal vector which is different from the unit tangential vector $\hat{\mathbf{e}}_t$ of the path at the point D. The time derivative of $\hat{\mathbf{e}}_t$ in (13) is also modified as

$$\dot{\hat{e}}_t = \frac{1}{\left|\hat{e}_n + (L/2\pi R_c)\hat{e}_{\text{rot}}\right|}\left(-\frac{1}{\left|\overrightarrow{R}_{\text{cm}}^{\perp}\right|}\left(\overrightarrow{V}_m \cdot \hat{e}_n\right)\hat{e}_d\right), \tag{26}$$

where L is a pitch of helix.

In this way, the motion of virtual target can be computed according to the geometry of the desired path. Therefore, the proposed guidance logic might be extendable to any smooth path.

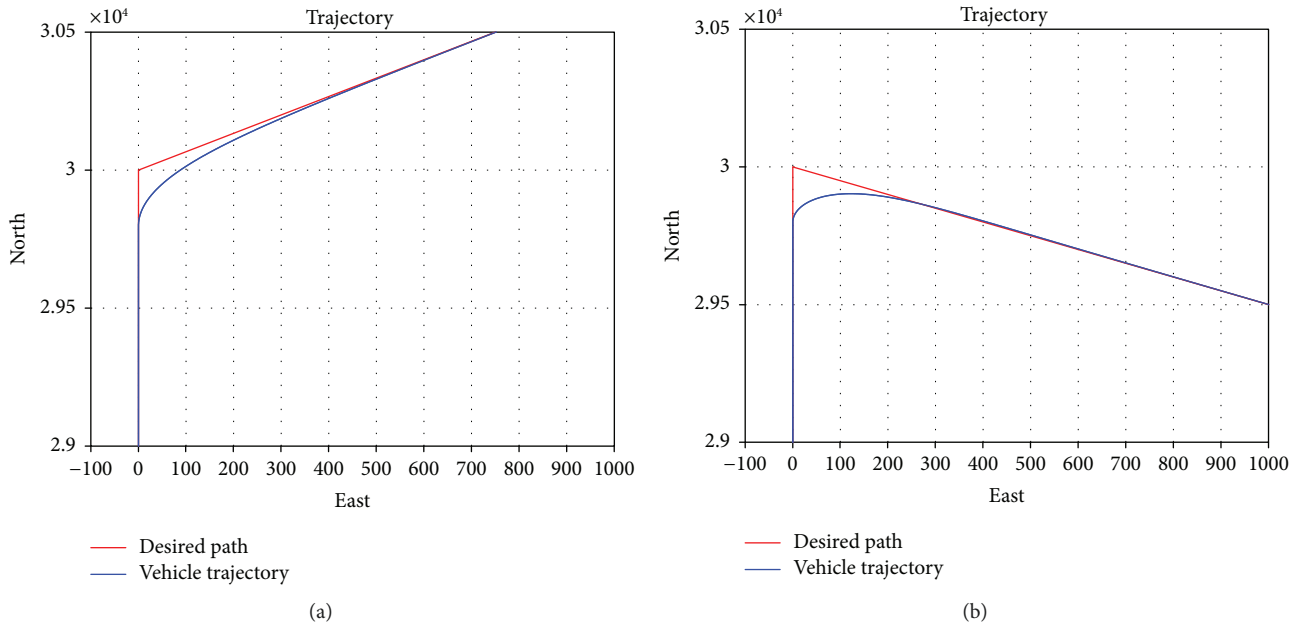

Figure 10: Path transition between straight-line segments. (a) Obtuse angle, (b) acute angle.

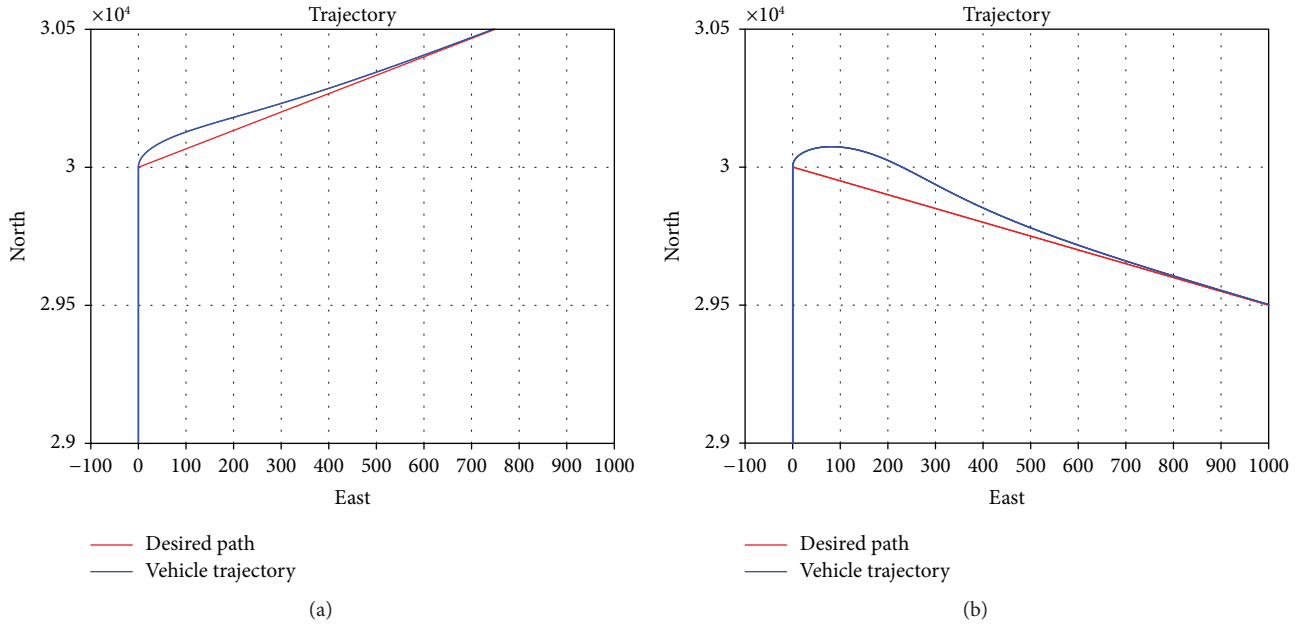

Figure 11: Path transition over the waypoint. (a) Obtuse angle, (b) acute angle.

Table 1: Initial conditions used in simulations.

Line colour	Initial positions (x: north, y: east, h: altitude in meters)	Initial headings ψ and flight path angles γ (deg)
Orange	$x = 50, y = 500, h = 300$	$\psi = 0, \gamma = 0$
Magenta	$x = 50, y = -500, h = 300$	$\psi = -90, \gamma = 30$
Blue	$x = 0, y = -500, h = 600$	$\psi = 0, \gamma = 60$
Green	$x = 100, y = -400, h = 800$	$\psi = 60, \gamma = -30$
Black	$x = 100, y = -500, h = 100$	$\psi = -30, \gamma = 0$

4. Simulations

In this section, the numerical simulations are performed to demonstrate the effectiveness of the proposed path following guidance logic. The path of a vehicle is defined in three dimensions and is assumed to be given to the vehicle a priori. It is also assumed that the vehicle is a point mass and is flying at a constant speed of 25 m/sec. The tangentially receding distance R_0 is chosen as 200 m, and $N = 1$ and $h = 2$ are used in simulations.

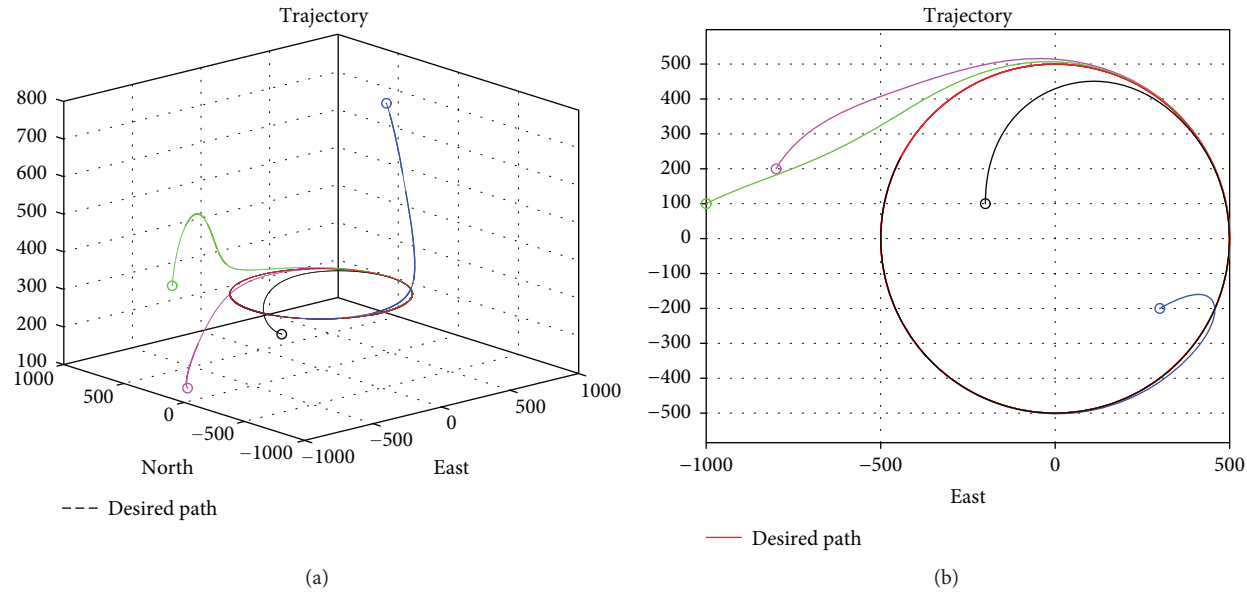

Figure 12: Circular path following. (a) Three-dimensional view, (b) planar view.

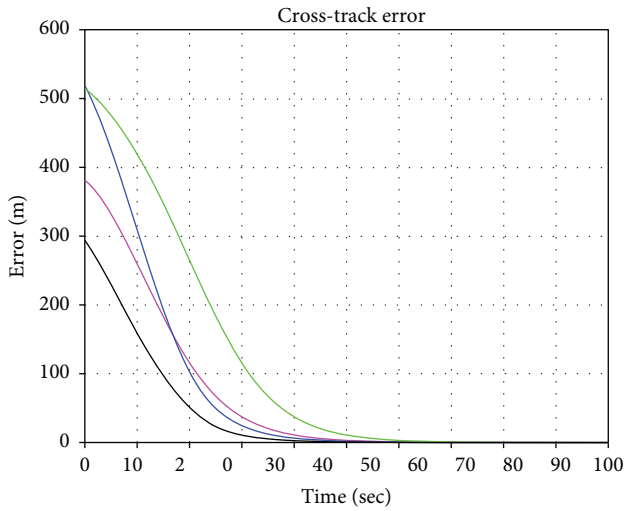

Figure 13: Cross-track errors.

To illustrate straight-line path following with the proposed guidance logic, three scenarios are considered, and the results are shown in Figures 8–11. In the first scenario, the vehicle begins at various initial positions and poses and is supposed to fly north along the desired straight-line path at an altitude of 300 m. The initial conditions used in the first scenario are summarized in Table 1. Figure 8 shows that the proposed logic can accommodate large deviations from the desired path, and the vehicle trajectory converges to the path without any following errors. The trajectories of cross-track error are shown in Figure 9.

As for the next two scenarios, Figure 10 illustrates the ability of the proposed guidance logic to follow straight-line path segments with both obtuse and acute angles. The receding distance R_0 detects the end of path segment, and the vehicle performs segment switching maneuver.

If the receding distance is longer, the vehicle will start its segment switching earlier. On the contrary, instead of using the receding distance, if the projection point D is used to detect the end of path segment, then over-waypoint transition is possible as shown in Figure 11. Although the transitions show some deviations around the waypoint, the vehicle returns to the next path segment without any following errors.

To illustrate circular path following with the proposed guidance logic, three scenarios are considered and the results are shown in Figures 12–15. In the first scenario, the vehicle begins at various initial positions and poses and is supposed to fly along circular path with the circle radius of 500 m at an altitude of 300 m. The initial conditions used in the first scenario are summarized in Table 2. Figure 12 shows that the vehicle trajectory converges to the desired circular path with any following errors. The trajectories of cross-track error are shown in Figure 13.

To further test the circular path following capabilities of the proposed guidance logic, two more scenarios are simulated. One is for oblique circular paths defined in three-dimensional space and the other is for path transitions between concentric circular paths. In Figure 14, it can be seen that the vehicle trajectories converge to an oblique circular path without any following errors, and Figure 15 shows the vehicle successfully transits and follows two concentric circular paths with varying radii and inclination angles.

Figure 16 illustrates how the proposed guidance logic can track a helical path with any following error. The helical path is defined on a vertical cylinder of radius 500 m, having pitch of $L = 10(2\pi)$m.

5. Conclusions

This paper presents a new simple and efficient three-dimensional path following guidance logic. The proposed

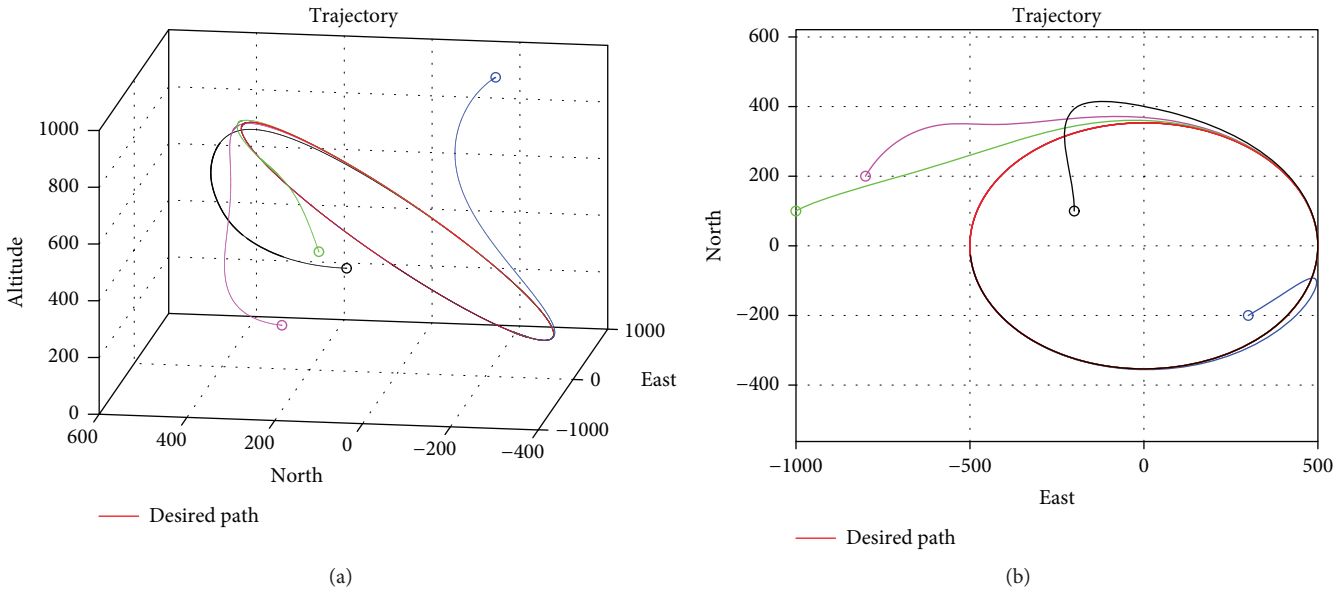

Figure 14: Path following with an oblique circle (with inclination angle of 45 degree). (a) Three-dimensional view, (b) planar view.

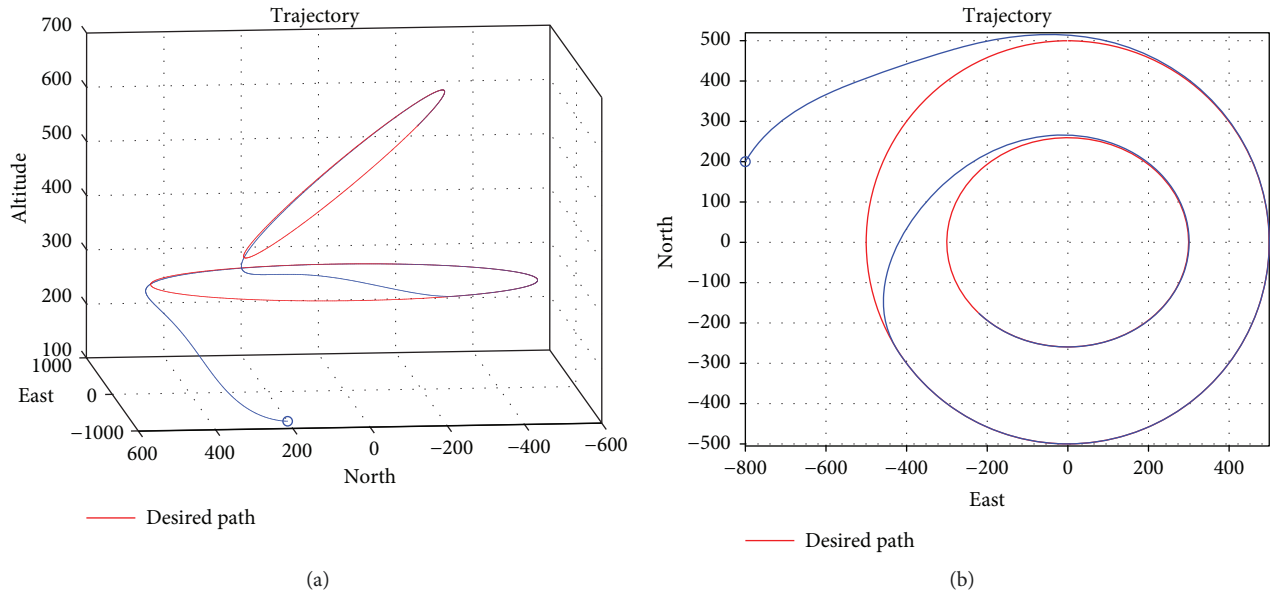

Figure 15: Circular path transition with circle radii of 500 m and 300 m and inclination angles of 0 and 30 degrees, respectively. (a) Three-dimensional view, (b) planar view.

Table 2: Initial conditions used in simulations.

Line colour	Initial positions (x: north, y: east, h: altitude in meters)	Initial headings ψ and flight path angles γ (deg)
Magenta	$x = 200, y = -800, h = 100$	$\psi = 30, \gamma = 0$
Blue	$x = -200, y = 300, h = 800$	$\psi = 60, \gamma = -30$
Green	$x = 100, y = -1000, h = 400$	$\psi = 60, \gamma = 60$
Black	$x = 100, y = -200, h = 200$	$\psi = 0, \gamma = 0$

guidance logic is composed of the guidance law and the motion strategy of the virtual target along the desired path.

As for the guidance law, the combined pure proportional navigation guidance (PPNG) and pursuit guidance (PG) are proposed. The combined law enhances damping for a straight-line path and provides the centripetal acceleration for a circular path. This guidance law makes a vehicle pursue the virtual target efficiently. As for the motion strategy of the virtual target, the motion is explicitly specified by introducing the concept of the projection point and the tangentially receding distance. Although more complex computations are expected than the straight-line or circular path, the

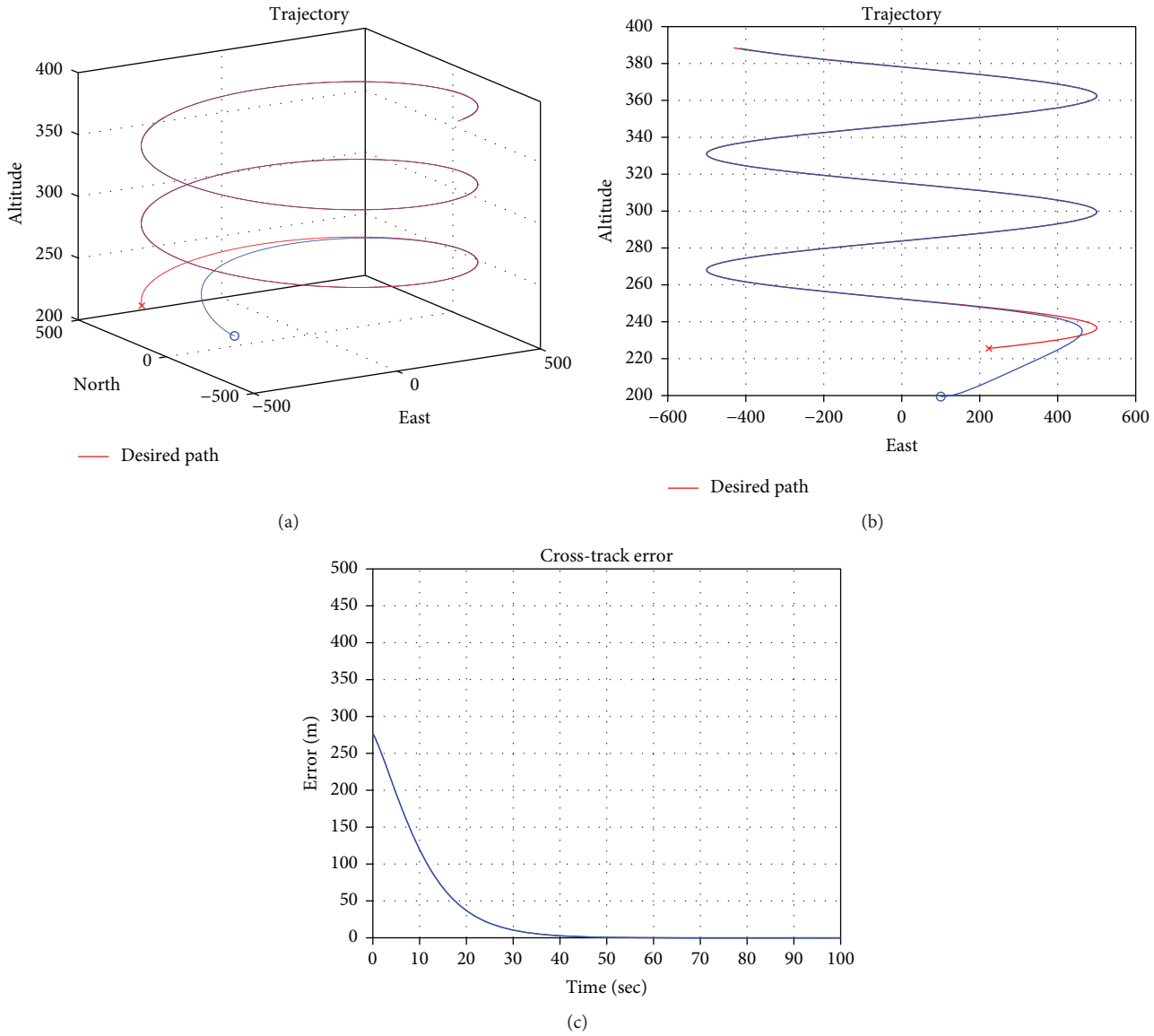

Figure 16: Helical path following. (a) Three-dimensional view, (b) side view, (c) cross-track error.

proposed guidance logic is conceptually extendable to any smooth path.

The effectiveness of the proposed logic has been demonstrated by the numerical simulations with various scenarios. For straight-line, circular, and helical paths defined in three-dimensional space, the proposed logic provides precise path following.

Data Availability

All data used to support the findings of this study are available from the corresponding author upon request.

Conflicts of Interest

The authors declare that there is no conflict of interest regarding the publication of this paper.

Acknowledgments

This work was supported by Sejong University.

References

[1] G. E. Franklin, J. D. Powell, and A. Emami-Naeini, *Feedback Control of Dynamic Systems*, Prentice–Hall, 2002.

[2] M. Rathinam and R. M. Murray, *Configuration Flatness of Lagrangian Systems Underactuated by Prentice–Hall*, Upper Saddle River, NJ, 2002.

[3] E. Johnson, A. Calise, and E. Corban, "A six degree-of-freedom adaptive flight control architecture for trajectory following," in *AIAA Guidance, Navigation, and Control Conference and Exhibit*, Monterey, California, August 2002.

[4] D. J. Gates, "Nonlinear path following method," *Journal of Guidance, Control, and Dynamics*, vol. 33, no. 2, pp. 321–332, 2010.

[5] D. R. Nelson, D. B. Barber, T. W. McLain, and R. W. Beard, "Vector field path following for miniature air vehicles," *IEEE Transactions on Robotics*, vol. 23, no. 3, pp. 519–529, 2007.

[6] D. A. Lawrence, E. W. Frew, and W. J. Pisano, "Lyapunov vector fields for autonomous unmanned aircraft flight control," *Journal of Guidance, Control, and Dynamics*, vol. 31, no. 5, pp. 1220–1229, 2008.

[7] V. Cichella, I. Kaminer, V. Dobrokhodov, E. Xargay, N. Hovakimyan, and A. Pascoal, "Geometric 3D path-following control for a fixed-wing UAV on SO(3)," in *AIAA Guidance, Navigation, and Control Conference*, Portland, Oregon, August 2011.

[8] T. Yamasaki, H. Takano, and Y. Baba, *Robust Path-Following for UAV Using Pure Pursuit Guidance*, Aerial Vehicles, InTech, 2009.

[9] S. Park, *Avionics and Control System Development for Mid-Air Rendezvous of Two Unmanned Aerial Vehicles, [Ph.D. thesis]*, MIT, 2004.

[10] S. Park, J. Deyst, and J. P. How, "A new nonlinear guidance logic for trajectory tracking," in *AIAA Guidance, Navigation, and Control Conference and Exhibit*, Providence, Rhode Island, August 2004.

[11] G. Ducard, K. C. Kulling, and H. P. Geering, "A simple and adaptive on-line path planning system for a UAV," in *2007 Mediterranean Conference on Control & Automation*, pp. 1–6, Athens, Greece, June 2007.

[12] E. D. B. Medagoda and P. W. Gibbens, "Synthetic-waypoint guidance algorithm for following a desired flight trajectory," *Journal of Guidance, Control, and Dynamics*, vol. 33, no. 2, pp. 601–606, 2010.

[13] J.-m. Zhang, Q. Li, N. Cheng, and B. Liang, "Nonlinear path-following method for fixed-wing unmanned aerial vehicles," *Journal of Zhejiang University Science C*, vol. 14, no. 2, pp. 125–132, 2013.

[14] P. Encarnacao and A. Pascoal, "Combined trajectory tracking and path following: an application to the coordinated control of autonomous marine craft," in *Proceedings of the 40th IEEE Conference on Decision and Control (Cat. No.01CH37228)*, vol. 1, pp. 964–969, Orlando, FL, USA, December 2001.

[15] P. Zarchan, *Tactical and Strategic Missile Guidance*, vol. 176, AIAA, 1997.

[16] S.-H. Song and I.-J. Ha, "A Lyapunov-like approach to performance analysis of 3-dimensional pure PNG laws," *IEEE Transactions on Aerospace and Electronic Systems*, vol. 30, no. 1, pp. 238–248, 1994.

[17] J.-H. Oh and I.-J. Ha, "Capturability of the 3-dimensional pure PNG law," *IEEE Transactions on Aerospace and Electronic Systems*, vol. 35, no. 2, pp. 491–503, 1999.